Journal of Chromatography A, 1422 (2015) 260–269

Contents lists available at ScienceDirect

Journal of Chromatography A

journal homepage: www.elsevier.com/locate/chroma

Application of Asymmetric Flow Field-Flow Fractionation hyphenations for liposome–antimicrobial peptide interaction

Patrizia Iavicoli[a], Patricia Urbán[a], Angelo Bella[b], Maxim G. Ryadnov[b], François Rossi[a], Luigi Calzolai[a,*]

[a] European Commission, Joint Research Centre, Institute for Health and Consumer Protection, I-21027 Ispra, VA, Italy
[b] National Physical Laboratory, Teddington TW11 0LW United Kingdom

ARTICLE INFO

Article history:
Received 13 July 2015
Received in revised form 8 October 2015
Accepted 9 October 2015
Available online 20 October 2015

Keywords:
Field-Flow Fractionation
Dynamic light scattering
Shape factor
Liposomes
Antimicrobial peptides

ABSTRACT

Asymmetric Flow Field-Flow Fractionation (AF4) combined with multidetector analysis form a promising technique in the field of nanoparticle characterization. This system is able to measure the dimensions and physicochemical properties of nanoparticles with unprecedented accuracy and precision. Here, for the first time, this technique is optimized to characterize the interaction between an archetypal antimicrobial peptide and synthetic membranes. By using charged and neutral liposomes it is possible to mimic some of the charge characteristics of biological membranes. The use of AF4 system allows determining, in a single analysis, information regarding the selectivity of the peptides, the quantity of peptides bound to each liposome, the induced change in the size distribution and morphology of the liposomes. The results obtained provide relevant information for the study of structure–activity relationships in the context of membrane-induced antimicrobial action. This information will contribute to the rational design of potent antimicrobial agents in the future. Moreover, the application of this method to other liposome systems is straightforward and would be extremely useful for a comprehensive characterization with regard to size distribution and protein interaction in the nanomedicine field.

1. Introduction

The size and morphology of nanosized objects is fundamentally linked to their properties. The need for a comprehensive size characterization of particles is critical in the field of nanomedicine. The lack of well-established, robust methods for measuring size and physicochemical properties of nanoparticles is hampering further application of nanotechnology in medicine.

Liposomes have a widespread use in nanomedicine [1] due to their bilayer construction mimicking biological membranes [2] and for their use as carriers for therapeutic agents [3,4]. In fact, several of the approved nanodrugs currently on the market are liposome-based drug delivery systems [5].

Among all the techniques used to characterize particles, AF4 is perhaps the most promising due to its flexibility to separate according to size a wide range of diverse particles [6]. The size-separated nanoparticles can then be directly analyzed by different detectors, thus giving access to a large variety of characterization possibilities. The combination of FFF with online multi angle light scattering (MALS) and dynamic light scattering (DLS) creates a powerful system for measuring the accurate particle size distribution in complex heterogeneous and polydispersed mixtures [7].

This technique is increasingly used on a routine basis in a variety of fields, including food, pharmaceuticals, water treatment, and chemical production [8–10]. In the field of nanomedicine AF4 helps to analyze small changes in size distribution or drug loading efficiency which are important aspects of quality control and essential for regulatory affairs and medical approval. AF4 has only a medium peak resolution, for example it can separate a mixture of silver nanoparticles of 40 and 70 nm in size [11], but it would have problems in separating particles with closer sizes.

In this study, AF4 is used to characterize liposomes and their interactions with antimicrobial peptides. Antimicrobial peptides are an important part of the innate immunity system to fight infection [12]. More than 1000 antimicrobial peptides (AMPs) have been discovered in various organisms including humans [13] and as the spread of antimicrobial resistance is no longer a future threat [14], there is a pressing need to develop novel classes of antimicrobial agents. AMPs are recognized as promising candidates in this regard [15]. The binding of AMPs to microbial membranes is facilitated by electrostatic interactions with bacterial membrane, rich in acidic phospholipids, which allows the hydrophobic

* Corresponding author. Tel.: +39 0332 786561; fax: +39 0332 789171.
E-mail address: luigi.calzolai@jrc.ec.europa.eu (L. Calzolai).

http://dx.doi.org/10.1016/j.chroma.2015.10.029

portions of the peptides to incorporate into the hydrophobic bilayer interfaces [16]. Electrostatic interactions can be viewed as a recognition or selectivity means since mammalian cell membranes are composed predominantly of zwitterionic phosphatidylcholine (PC) and sphingomyelin phospholipids [17]. These binding events define the mechanism of action of AMPs. To understand these mechanisms in sufficient detail model membranes that can mitigate the complexity of biological membranes while mimicking their physicochemical characteristics are necessary. Here we used liposomal unilamellar vesicles as model systems for elucidating peptide–membrane interactions relevant to antimicrobial activity. Two types of liposomes were used, anionic and neutral, to mimic microbial and mammalian membrane lipids, respectively. The liposomes give straightforward fluid-phase membranes at room and physiological temperature thus presenting ideal models for probing relevant peptide–membrane interactions [18].

In this paper, we show that by means of AF4 hyphenated to MALS, DLS, UV and Fluorescence spectroscopy detectors, it is possible to analyze particle size distribution and essential physicochemical properties pertaining to the membrane interactions of antimicrobial peptides in unprecedented detail.

2. Materials and methods

2.1. Materials

Lipids dilaurylphosphatidylcholine (DLPC), dilaurylphosphatidylglycerol (DLPG), palmitoyloleoylphosphatidylcholine (POPC) and palmitoyloleoylphosphatidylglycerol (POPG) were purchased from Avanti® Polar Lipids, Inc.

Salts used for the preparation of the mobile phase (monosodium phosphate monohydrate and disodium phosphate dihydrate) were purchased from Sigma–Aldrich.

The water used in this work was ultrapure water (prepared by Milli-Q®, Millipore S.A.) and was filtered through a membrane filter with a pore size 0.22 μm prior to use.

2.2. Preparation of membrane models (liposomes)

Unilamellar vesicles consisting of POPC and POPC/POPG (3:1 mole ratio) were prepared by dissolving the lipids in a chloroform:methanol (2:1, v:v) mixture at a concentration of 10 mg/mL. The solution was then evaporated under nitrogen flow overnight. The dried film was then resuspended in 10 mL of a 10 mM phosphate buffer, pH 7.4. The preparation was alternatively vortexed for 2 min and sonicated at room temperature for 2 min. The cycle was repeated three times. The dispersion was extruded 21 times through a 100-nm polycarbonate membrane before each use.

Vesicles consisting of DLPC and DLPC/DPLG (3:1 mole ratio) were prepared following the same procedure as described above.

2.3. Peptide synthesis

All peptides were assembled on a Liberty microwave peptide synthesizer (CEM Corp) using Rink Amide MBHA resin, standard solid-phase Fmoc/tBu protocols and HBTU/DIPEA as coupling reagents. An additional β-Ala residue was introduced at the N-termini of AmP and nAmP to act as a spacer prior fluorescein labelling. Fluorescein coupling was performed on solid phase using 5(6)-carboxyfluorescein, HBTU/DIPEA in a fourfold excess fashion over the total amount of peptide. Following cleavage and deprotection (95% TFA, 2.5% TIS, 2.5% water) peptides were purified using RP-HPLC and their purities were confirmed by analytical RP-HPLC and MALDI-ToF. The purity of all peptides was higher than 95%. Both analytical and semi-preparative RP-HPLC were performed using a JASCO HPLC system equipped with Vydac C18 columns (respectively 5 μm, 4.6 mm × 250 mm for the analytical and 5 μm, 10 mm × 250 mm for the semi preparative). Both analytical and semi preparative were run using a 10–60% B gradient over 46 min at 1 mL/min and 4.7 mL/min respectively with detection at 214 and 280 nm. Buffer A 5% and buffer B 95% acetonitrile in water with 0.1% TFA.

MS $[M+H]^+$: AmP m/z 2534.64 (calc.), 2535.58 (observed); nAmP m/z 2371.20 (calc.), 2370.95 (observed); F-AmP m/z 2963.68 (calc.), 2964.07 (observed); F-nAmP m/z 2800.24 (calc.), 2801.73 (observed);

2.4. Preparation of lipid to peptide (L/P) mole ratios

Amp and nAmP peptide solutions at 0.5 mM were prepared fresh before each experiment in 10 mM phosphate buffer, pH 7.4. The concentration was calculated by reading UV–vis absorbance at 280 nm due to the presence of a single aromatic residue (Y) in both peptides. For all experiments the lipid concentration of liposomes was kept constant at 1.2 mM for all liposome–peptide complexes studied. For a desired L/P ratio (mole), a 250 μL peptide aliquot at a defined concentration (from 120 μM to 16 μM) was added immediately before the measurements to 750 μL of a 1.6 mM liposome solution. The final volume of each sample solution was 1 mL.

2.5. Dynamic light scattering and Z potential analysis

The particle size distribution and the *Z*-potential were measured using a Malvern Zetasizer Nano-ZS instrument. Each sample had a volume of 500 μL in a PMMA cuvette and each measurement was done at 25 °C in triplicate. The refractive index of liposomes used was 1.45, the absorption coefficient was 0.001.

The number of data sets of each measurement was automatically optimized by the instrument according to the quality of the sample and the intensity of the scattered light (ideally the correlogram should have amplitude around 0.8). The data was analyzed using the manufacturer's Dispersion Technology Software (DTS version 7.01), using both the cumulant (single exponential) and multimodal analysis (multi exponential-Malvern, DTS algorithm). From the cumulant analysis, the value of hydrodynamic diameter (Zave (d.nm)) and polydispersity index (PdI) could be obtained. If the PdI was greater than 0.5, the hydrodynamic radius was calculated from the multimodal analysis. The instrument calibration was checked by using varied sizes of Polystyrene latex (PSL) beads standards.

Zetasizer flow mode measurements were performed in a Hellma Quartz Suprasil 3 mm flow-through cuvette adjusted to 3.90 mm measurement position and attenuator of 11. The temperature was adjusted at 25 °C.

For both flow and batch mode measurements were performed at the 173° backscattering angle.

2.6. Analytical set up of Asymmetric Flow Field-Flow Fractionation (AF4) system

Characterization of peptide–liposome complexes was carried out using an AF4 system (AF2000 Postnova Analytics, Germany). The channel used was 29 cm long with a spacer of 350 μm, a regenerated cellulose membrane with a 10 kDa cutoff was used. The flows were provided by two separate pumps and the cross-flow was realized by a separate piston pump which is continuously adjustable. The eluent was phosphate buffer solution 10 mM, pH 7.4 and was degassed by sonication with a water bath sonicator and with a vacuum degasser just before delivery. The flow was kept at 0.5 mL/min. Optimal separation of the liposomes was achieved using an injection flow of 0.20 mL/min and a constant cross-flow of degassed buffer solution of 1 mL/min for the first 5 min. A power gradient 1–0.1 mL/min for the next 60 min was applied and then a

constant 0.1 mL/min for the next 10 min. The output from the channel was connected online to a 18-angle static light scattering detector MALS (Dawn EOS, Wyatt Technology, Santa Barbara, CA, USA), to a UV–vis spectrometer (SPD-2a AV, Postnova Analytics) set at 500 nm wavelength for detection of the fluorescein labeled peptide, to a fluorimeter (RF-20A XS) set at 500 nm excitation wavelength and 522 nm emission wavelength for the detection of the fluorescein labeled peptide and to a DLS (Zetasizer Nanos S, Malvern Instruments Ltd.) for size determination. The injection volume was 20 μL.

Data acquisition was carried out by AF200 control software version 1.1.1.26 (Postnova Analytics) and Zetasizer software v 6.01 (Malvern Instruments Ltd).

MALS data acquisition and procession was performed using Astra 6.1.1.17 (Wyatt Technology). The geometric radii (R_G) of the liposomes were calculated using the data from 18 angles from the MALS detector applying the coated sphere model [19]. For the coated sphere model, the coat thickness, refractive index of the coat and refractive index of the medium need to be specified. Coat thickness was specified with 3.7 nm [20], the refractive index of the coat was 1.45[21], the refractive index of the medium was 1.333.

Coated sphere model was chosen among other fitting methods also because it gave the best quality fit in terms of fit error.

The UV–vis detector was calibrated in order to later translate the area of the FFF-UV–vis peak into a concentration. The calibration of the online UV–vis detector was obtained by injecting increasing amounts of F-AmP peptide in the FFF system without cross flow. The area under the curve of the UV signals was plotted against the concentration of peptide used. The equation obtained from fitting the data was used to calculate the total concentration of peptide bound to the liposomes.

2.7. Counting liposome concentration by qNano

Measurements were made using the qNano system obtained from Izon Science (Christchurch, New Zealand) incorporating the fluid cell, stretching apparatus, data recording, and analysis software (Version 3.1). Samples were prepared by diluting the stock liposome dispersion (2.5 mM lipid concentration in phosphate buffer) in PBS 2x to 1:100. Each sample was run in triplicate. The pulse signal was calibrated with a 100 nm polystyrene particle standard supplied by Izon Science. The pores used were designated "NP200" by the manufacturer and are described as the most suitable for detecting particles in the range of 100–300 nm. The macroscopic stretch applied to the membrane was 44 mm. An appropriate voltage (0.3 V) was selected for all experiments to enable the detection of the peaks above the level of noise (<10 pA). This was judged to be adequate when the peak magnitude was greater than 0.12 nA. 7 cm H_2O of pressure was applied to the top fluid cell using Izon's variable pressure unit to help facilitate the translocation of particles through the elastic pore. Typically, a bandwidth filter of 1 kHz was applied during measurements, and modal values from data histograms were used in all plots. In all experiments, 80 μL of electrolyte buffer was placed in the lower fluid cell. The volume in the upper fluid cell was 40 μL. After recording, this solution was withdrawn, and the fluid cell and pore were washed by repeatedly replacing PBS in the upper fluid cell until no particles were apparent on the signal trace. To generate error bars in all figures, the mean and standard deviation of three repeat experiments was used.

2.8. Negative stained transmission electron microscopy

TEM images were taken with a JEOL JEM 2100 TEM microscope at 200 keV.

The negative stain used was 1% of uranyl acetate dissolved in distilled water (pH 4.5). The stain was filtered through a 0.22 μm filter that had been pre-rinsed with large volumes of distilled water. The filtered stain was stored in the dark at 4 °C.

Liposome dispersion was diluted to 0.5 mg of lipid/mL. One drop of this dispersion was placed on a glow discharged 200-mesh formvar copper grid, allowed to adsorb for 3 h at 4 °C and the surplus was removed by filter paper. The grid was then placed on top of the surface of a drop of 1% uranyl acetate for 1 min and the excess removed with filter paper. The grid was dried in a desiccator at room temperature and examined the day after.

2.9. Theoretical isoelectric points

The theoretical isoelectric point of AmP and n-AmP peptides were computed from ExPaSy Bioinformatics Resource Portal (http://web.expasy.org/compute_pi/).

3. Results and discussion

3.1. Liposomes as bacterial and mammalian membrane mimetics

Different liposomes were assembled using 4 different phospholipids: palmitoyloleoylphosphatidylcholine (POPC), palmitoyloleoylphosphatidylglycerol (POPG), dilaurylphosphatidylcholine (DLPC), and dilaurylphosphatidylglycerol (DLPG). The phospholipids carrying the choline terminal head group are neutral (POPC, DLPC), while those carrying the glycerol head group are negatively charged (POPG, DLPG). In addition, the dilauryl and palmitoyloleoyl aliphatic chains differ in length (C12 vs. C18, respectively), resulting inmembranes of two thicknesses which, together with a double bond in the palmitoyloleoyl chain, renders the PO-type membranes thicker and less fluid [22].

3:1 molar ratios of neutral and negatively charged phospholipids gave Anionic Unilamellar Vesicles (AUVs). Zwitterionic Unilamellar Vesicles (ZUVs) were assembled from the neutral lipids only. The total of four liposomes provided model systems mimicking the negatively and neutrally charged membrane lipids, respectively [17].

3.2. Size distribution of liposomes by DLS

The size and polydispersivity of the four different liposomes were measured by DLS. The *Z*-average particle diameter of PO- and DL-AUVs, PO- and DL-ZUVs was 124, 108, 156 and 107 nm respectively. The polydispersivity represented by the PdI value was less than 0.15 for all samples analyzed, thus confirming the homogeneity of the different liposomes after extrusion. These values are comparable with the ones found in literature, where large unilamellar vesicles, prepared by extruding lipid dispersion trough polycarbonate filters of 100 nm, have a size of 120–140 nm [23]. The DLS data indicates that liposomes formed by lauryl alkyl chains have slightly smaller size than liposomes containing the palmitoyl chain. These results are consistent with the shorter C12 chain present in the DL-type samples compared to the C18 chain present in the PO-type ones. The *Z*-potential was measured in phosphate buffer at pH 7.4 as -70.3 ± 11.5, -64.9 ± 11.7, -10.1 ± 6.9, -12.5 ± 7.4 mV for PO- and DL-AUVs, PO- and DL-ZUVs respectively. These data confirm that AUVs and ZUVs have negative and neutral electric potential respectively.

3.3. Size distribution of liposomes by AF4-DLS system

Dynamic light scattering cannot provide an adequate measure of polydispersed samples, containing mixtures of nanoparticles which have less than a factor of 3 size difference [24]. To overcome some

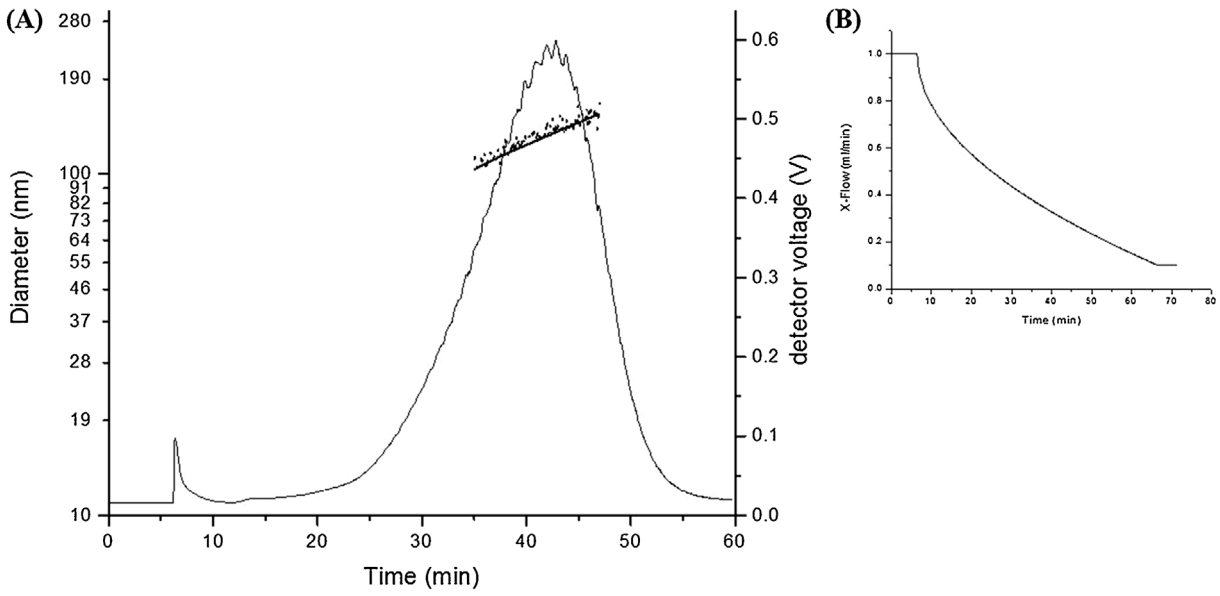

Fig. 1. AF4-MALS-DLS analysis of PO-AUVs. (A) Fractogram showing the light 90° scattering detector signal (right hand scale), gyration diameter (continuous line, left hand scale, logarithmic scale) calculated from AF4-MALS data using the coated sphere fitting method and hydrodynamic diameter (dotted line, left hand scale, logarithmic scale) reporting the DLS *Z*-average values. (B) Cross flow method used for the AF4 separation.

of these drawbacks, we analyzed the liposomes with AF4 coupled online with MALS, DLS and UV detectors (AF4-MALS-DLS-UV). A representative example of AF4-MALS-DLS analysis for PO-AUVs is shown in Fig. 1A. The fractogram (90° light scattering detector) shows the presence of a broad peak centered at 42 min exit time which suggests the presence of particles of a definite size range. The online MALS and DLS detectors allow the direct measurement of both the gyration diameter [25] (continuous line in Fig. 1A) and the hydrodynamic diameter (dotted line in Fig. 1A) of the liposomes exiting the AF4 separation channel.

The fractogram and the monotonic increase of the particle size with the exit time (Fig. 1A) indicate that the cross flow solvent (phosphate buffer 10 mM, pH 7.4) and the cross flow method used (starting at 1 mL/min and decreasing to 0.1 mL/min with a power gradient, Fig. 1B) was optimal to achieve a satisfactory separation of the polydispersed PO-AUVs. This method provides an ideal compromise between achieving good separation over a wide range of sizes, while keeping the overall experiment time reasonable. In order to evaluate the adsorption of the liposomes to the accumulation wall during size separation, the total amount of particles eluting from the channel with and without cross-flow was calculated comparing the area under the curve (AUC) of the UV signals. It was found that the AUC was the same with and without separation. This indicates that the AF4 separation method used in this study did not cause any liposome retention inside the channel. The AF4-DLS data for PO-AUVs thus shows the presence of liposomes with sizes comprised between 90 and 150 nm, with a peak at 123 nm. Similar measurements gave hydrodynamic diameters at the peak maximum of 110, 151, 104 nm for DL-AUVs, PO- and DL-ZUVs, respectively in excellent agreement with the *Z*-average values obtained by DLS in batch mode.

3.4. Shape factor of liposomes by AF4-MALS-DLS system

The availability of the online MALS and DLS data allows determining the morphology of the particles by calculating the shape factor (given by the R_G/R_H ratio, ρ [26]). The use of the shape factor for shape determination has been reported for both macromolecules [27–29] and nanoparticles [30–33]. To determine the particle size and shape of the liposomes, different fitting methods for light scattering data retrieved from MALS were evaluated. The comparison between the different fitting models showed that the coated sphere model gave the best fitting results and was more suitable to describe our data than any other geometry. The R_G/R_H ratios were calculated for PO-AUVs between 35 and 47 min. The shape factor was found to be quite constant along the particle size distribution (**Fig. A-1**). Rigid spheres nanoparticles (where the mass has an homogenously distribution) have predicted shape factor values of 0.775, coated spheres (where the mass is concentrated on a thin layer on the external surface) have ρ values close to 1, while oblong nanoparticles (such as nanorods, nanotubes or nanofibers) would have ρ values larger than 1 [34]. Thus, our results with ρ values close to 1, show that PO-AUVs have the morphology of a coated sphere and a size distribution comprised between 90 and 150 nm; furthermore, their shape is kept constant and unaltered during the AF4 separation. These results are consistent with previous observations that the coated sphere model is the best fitting method for liposomes [19,35].

Similarly, at the maximum of the AF4-LS 90° peak, the ρ values for PO- and DL-AUVs are 1.04 and 0.95 respectively. This indicates that the liposomes under study have coated sphere morphology and do not change their spherical shape during the duration of the whole analysis.

3.5. Characterization of liposome–peptide complexes

3.5.1. Size distribution by DLS

Once optimized, the methods were used to characterize the size distribution and morphology of our cell membrane mimics interacting with a *de novo* designed archetypal antimicrobial peptide. For the purpose of the study two synthetic peptides were investigated – a positively charged antimicrobial peptide (AmP) and its anionic,"mirror", non-antimicrobial counterpart (nAmP). AmP interacts with the negatively charged bacterial membrane, while the nAmP does not.

The peptides (whose exact sequence will be reported elsewhere) were assembled according to the previously published principles [36,37]. More specifically, the 21 amino acids polypeptide has a generic sequence – PNPHNPHPNPHNPHPNPHNPH – where P – polar; N – neutral, polar or small; H – hydrophobic. When

Table 1
Size measurement by DLS in batch mode of PO-AUVs, ZUVs and DL-AUVs, ZUVs after addition of either the peptide AmP or the peptide nAmP at variable L/P mole ratios. The size is the *Z*-average of the hydrodynamic diameter and it is expressed in nm. The PDI of all measurements is less than 0.15.

	Liposome alone	100:1	80:1	60:1	40:1	20:1
PO-AUV/AmP	124.2 ± 1.1	122.6 ± 0.9	121.8 ± 0.3	120.5 ± 1.2	Increased Scattering	Increased Scattering
PO-AUV/nAmP	124.2 ± 1.1	124.1 ± 0.3	123.3 ± 0.6	124.1 ± 1.9	123.5 ± 1.2	122.7 ± 0.8
PO-ZUV/AmP	156.1 ± 1.1	153.8 ± 0.8	155.5 ± 0.6	152.4 ± 1.4	153.6 ± 1.6	154.5 ± 1.3
DL-AUV/AmP	108.1 ± 0.1	134.4 ± 2.4	135.2 ± 1.7	137.2 ± 1.5	148.6 ± 0.9	Increased Scattering
DL-AUV/nAmP	108.1 ± 0.1	110.6 ± 1.1	114.1 ± 1.5	111.4 ± 1.3	112.3 ± 1.8	111.7 ± 0.7
DL-ZUV/AmP	106.7 ± 0.9	107.2 ± 1.1	107.5 ± 0.7	105.8 ± 1.1	106.2 ± 0.4	107.2 ± 0.8

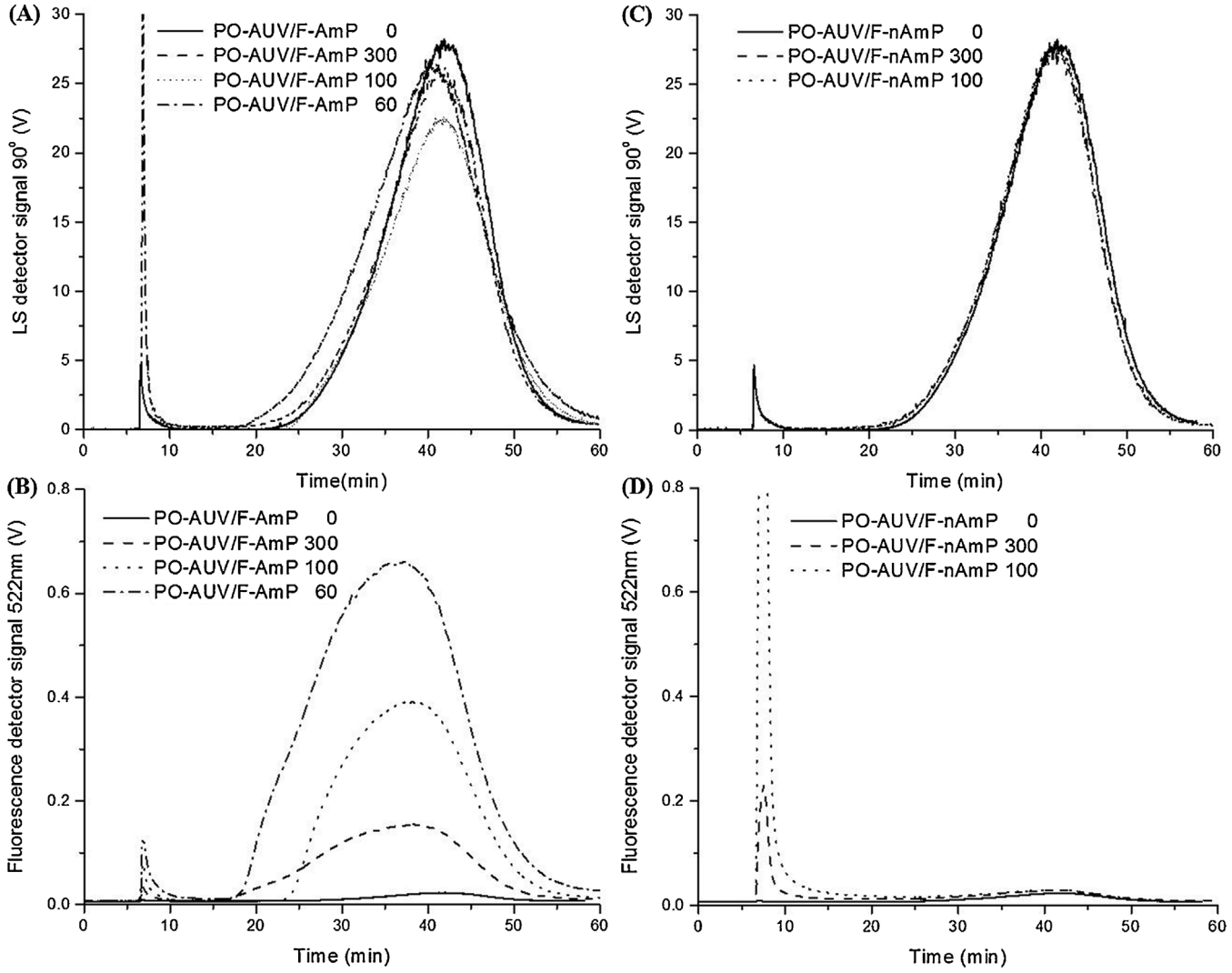

Fig. 2. Separation by AF4 and analysis by 90°-LS and fluorescence detectors (500 nm excitation and 522 nm emission). (A and B) PO-AUVs mixed with F-AmP at variable L/P mole ratios. (C and D) PO-AUVs mixed with F-nAmP at variable L/P mole ratios. The concentration of liposomes is fixed.

the "P" amino acids are positively charged the resulting molecule (AmP, molecular weight 2535 Da) has an isoelectric point of 12.3. Upon binding to negatively charged phospholipid bilayers the AmP peptide forms an amphipathic helix, with polar and hydrophobic residues segregating into polar and hydrophobic faces. In the case of "P" being negatively charged, the molecule (nAmP, molecular weight 2371 Da) has an isoelectric point of 3.5. Thus, while having identical hydrophobic faces, AmP and nAmP have oppositely charged (cationic and anionic) polar faces.

The peptides also accommodate specific experimental requirements such as the presence of a single tyrosine (Y) residue to facilitate accurate concentration determination by UV. The adoption of the peptide α-helical structure was confirmed by circular dichroism experiments after mixing AmP with both PO- and DL-AUVs (data not shown).

In order to follow the change in the hydrodynamic diameter of each liposome upon addition of increasing amounts of both polypeptides we used DLS in batch mode. This change was used as an indicator of the affinity and penetration of the peptide with the membrane. Table 1 compares the size of bare liposomes with the size of the complex formed after addition of peptides at different lipids to peptide (L/P) mole ratios.

This simple experiment allowed identifying the point at which further addition of peptide disrupted the stability of the liposomes. That point was reached at L/P mole ratio of 40:1 for PO-AUVs/AmP and at L/P mole ratio of 20:1 for DL-AUVs/AmP when

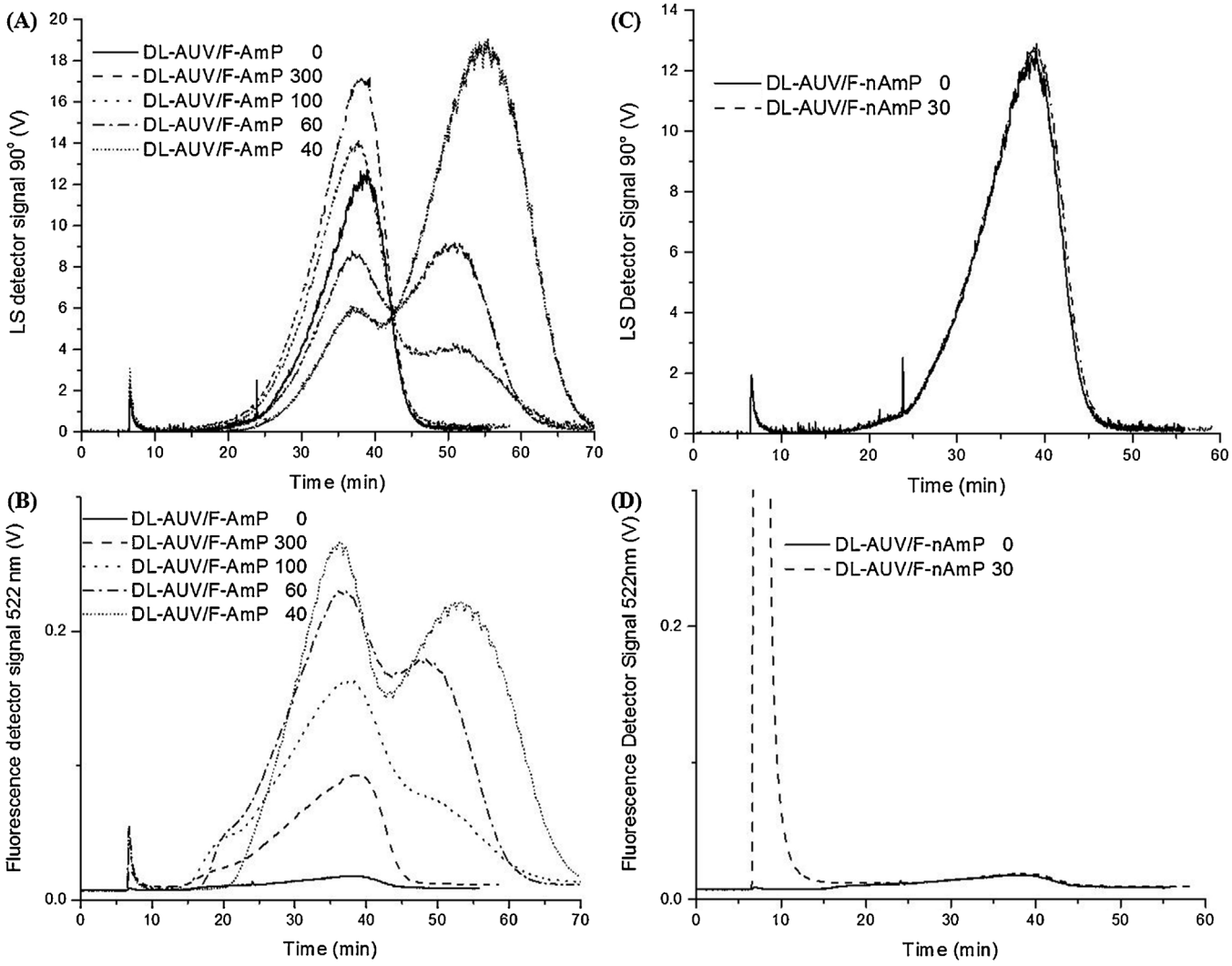

Fig. 3. Separation by AF4 and analysis by 90°-LS and fluorescence detectors (500 nm excitation and 522 nm emission). (A and B) DL-AUVs mixed with F-AmP at variable L/P mole ratios. (C and D) DL-AUVs mixed with F-nAmP at variable L/P mole ratios. The concentration of liposomes is fixed.

the liposomes collapsed as judged by larger sizes and broader size distributions.

As measured by DLS, liposomes alone are stable up to 1 month if stored protected from light at 4 °C. As regarding the liposome/peptide complexes, PO-AUV/AmP are stable up to L/P mole ratio 60:1, whereas DL-AUV/AmP are stable up to L/P mole ratio 100:1. Lower ratios of these complexes show aggregation by DLS after 24 h.

The DLS data shows that for almost all samples, there is no significant change in size (as measured by batch mode DLS) upon addition of AmP and nAmP peptides to the different liposomes. The only significant change in the hydrodynamic diameter of the complex is detected in the case of DL-AUVs/AmP system that shows an increase from around 110 nm for the free liposome to around 140 nm for the complexes.

The formation of a layer of peptides around the liposomes would increase minimally the diameter of the liposome–peptide complex and thus could not be detected by DLS in batch mode.

3.5.2. *Peptide binding specificity by AF4-MALS-Fluorimeter system*

To better characterize peptide–liposome interactions, we coupled the AF4 separation unit with online fluorescence detector in order to obtain a peptide-specific signal. Fluorescence of a tyrosine residues present in each peptide was not sufficient to detect peptides at such used concentrations, therefore the carboxyfluorescein (F) was attached to the N-terminus of each peptide via a beta-alanine spacer, termed F-AmP and F-nAmP, allowing detection by fluorometer and UV detectors.

All four membrane models alone and mixed with cationic and anionic peptides at different L/P ratios were analyzed using the AF4-MALS-Fluorimeter-UV system. The concentration of liposomes was kept constant at 1.2 mM. Fig. 2 shows the AF4 analysis (90° light scattering and fluorescence detectors) of the PO-AUVs mixed with increasing concentrations of F-AmP (Fig. 2A and B) and F-nAmP peptides (Fig. 2C and D). The fractograms obtained with the scattering detectors (Fig. 3A and C) show only one broad peak centered at 42 min exit time, which is attributed to the liposomes. The retention time and the intensity of the peaks for all samples are quite similar to each other, showing no significant change in dimensions and concentrations upon addition of peptide to the liposomes.

The fluorescence detector clearly shows the binding of F-AmP to the PO-AUVs (Fig. 2B). The data indicates that the maximum fluorescence is reached for particles at exit time of around 40 min and that the integral of the fluorescence signal increases linearly with an increasing amount of fluorescent peptide. By contrast, F-nAmP peptide does not cause any increase in fluorescence (Fig. 2D), while

none F-AmP and F-nAmP is able to bind to the neutrally charged PO-ZUVs (data not shown).

These results confirm that F-AmP selectively binds to the negatively charged PO-AUVs, while the negatively charged F-nAmP does not interact with either negative or neutral liposomes.

The experimental data suggest a model for the peptide-liposome complex AmP-AUV: the peptide interacts with the liposomes by electrostatic interactions. Upon binding, the peptide folds into an amphipathic α-helix with a polar and a hydrophobic face, which favors the interaction with the hydrophobic part of the phospholipid molecules.

Similar results could be expected when repeating the experiments with both the DL-AUVs and ZUVs, even if the addition of F-AmP to the negative liposome causes an increase in size of the resulting complex (Table 1). Quite surprisingly, Fig. 3A shows that the addition of F-AmP to DL-AUVs results in the formation of a second peak in the FFF-LS fractogram compared to the liposomes alone.

The data indicates that the addition of F-AmP to DL-AUVs causes the formation of two well-defined liposome/F-AMP complexes: the first one with the same size of a free DL-AUVs and the second one with a larger size. With the increasing amount of F-AmP, the population of the smaller complex decreases, while the population of the bigger one increases. In addition, the fluorescence data (Fig. 3B) shows that the F-AmP peptide indeed binds to both small and large particles. By contrast, the addition of F-nAmP to DL-AUVs does not cause the appearance of a second peak in the FFF-LS fractogram (Fig. 3C) and the fluorescence data (Fig. 3D) shows that the peptide does not bind, as expected, to the liposomes. Similarly, no signal change was observed for the DL-ZUVs/F-AmP complexes (data not shown).

3.5.3. Size distribution by AF4-UV-DLS system

To measure the size of the two complexes in the DL-AUVs/F-AmP system, the hydrodynamic diameter was recorded by DLS on-line after the AF4 separation step. Fig. 4 shows the AF4-UV–vis fractogram obtained by recording at 500 nm (the absorbance maxima of the fluorescent-labeled F-AmP peptide) and the particle diameter (obtained by online DLS) for the free DL-AUVs (red line and dots) and the complex at L/P ratio 40. The data indicate that the smaller DL-AUVs/F-AmP complex does not change the size of around 110 nm compared to free liposomes and that the bigger complex has a size of around 180 nm. Similar experiments using

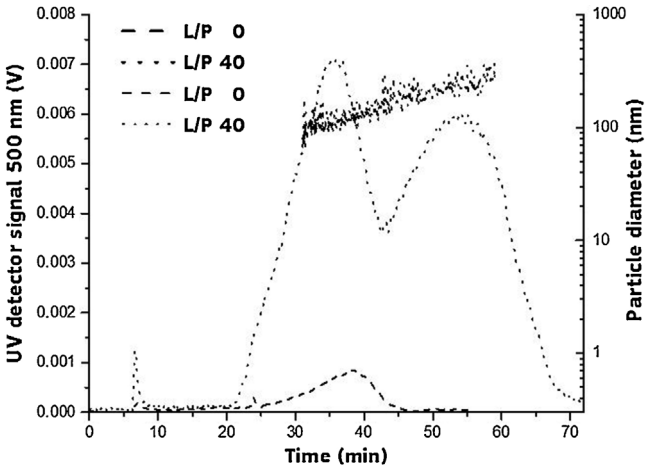

Fig. 4. Separation by AF4 and size measurement by DLS online of liposomes DL-AUVs alone and mixed with the F-AmP peptide at L/P mole ratio 40. Fractograms showing the UV detector signal (left hand scale), hydrodynamic diameter (dotted line, right hand scale, logarithmic scale) reporting the DLS *Z*-average values.

Table 2
Quantification of the concentration of F-AmP peptide bound to the liposomes. Percentage of peptide bound to liposomes PO-AUVs amd DL-AUVs at variable L/P mole ratios.

	600:1	300:1	100:1	80:1
PO-AUV/F-AmP	95.0 ± 1.6	64.3 ± 5.8	54.9 ± 4.0	49.0 ± 2.7
DL-AUV/F-AmP	106.8 ± 15.4	86.7 ± 8.6	66.9 ± 4.0	64.1 ± 3.7

AF4-DLS for the complexes PO-AUVs/F-AmP show no measurable size increase compared to liposomes alone (data not shown).

Thus, the increase in size measured by DLS in batch mode (Table 1) for DL-AUVs/F-AmP complexes is in reality caused by the presence of an additional population of larger complexes. These results highlight the well-known difficulty of DLS measurements in resolving particles which have less than a factor of 3 size difference and the fact that the intensity of the scattered light is inversely proportional to sixth power of the radius of the nanoparticle [38–40]. All these considerations highlight the importance of verifying the "real" size of particles present in the sample by a method that separates particles based on their size, like the AF4 system used herein.

The data of Fig. 4A and B allow estimating the relative number of peptides bound to the two DL-AUVs/F-AmP complexes. In fact, at L/P ratio of 80, the integrals of the light scattering peaks of complex 1 (size 110 nm) and complex 2 (size 180 nm) are equal; Considering that the intensity of the scattered light scales as R^6 it can be concluded that complex 1 contains 32 times the number of particles of complex 2. On the other hand, the integrals of fluorescence peaks for complex 1 and complex 2 are in a 60 to 40 ratio. Thus, each particle of complex 2 binds approximately 20 times more peptides than complex 1, while based on total surface area considerations it should bind only 4 times more peptides. This phenomenon was not observed for thicker and less fluid PO-AUVs that formed a single main peak upon peptide interaction [41].

3.5.4. Quantification of peptides bound to liposomes by AF4-UV system

The use of the fluorescently labeled peptides allowed quantifying the amount of peptides bound to liposomes by either using the UV–vis or fluorescence detectors. We have noticed that while the fluorescence detector is around 10 times more sensitive, the UV–vis data are more reproducible and the response vs. concentration of labeled peptide is more linear than fluorescence data, thus we have used the UV–vis data for quantification. By plotting the different concentrations of F-AmP used in the mixtures with both AUVs models against the AUC of the UV signals, it could be observed that the intensity of UV signals increased linearly with the peptide concentration (**Fig. A-2**).

In order to later translate the area of the FFF-UV–vis peak into a concentration, the calibration of the UV detector was performed and the resulting equation used to calculate the percentage of the bound peptide with respect to the total amount of peptide used at different L/P ratios for both PO-AUVs/F-AmP and DL-AUVs/F-AmP complexes (Table 2).

By plotting the percentage of peptide bound to liposomes towards the L/P mole ratios (Fig. 5), it could be observed that, for both liposome models, the percentage of bound peptide with respect to the total amount added decreases by increasing the total amount of peptide. The data seems to reach a plateau at around 60% of bound peptide for L/P ratio 80. Reporting the data as bound peptides per liposome versus free peptide per liposome and fitting to a Hill-type equation (Fig. A-3) gives a maximum number of bound peptides of 12000 and suggest a non-cooperative binding behavior (see supporting information for details).

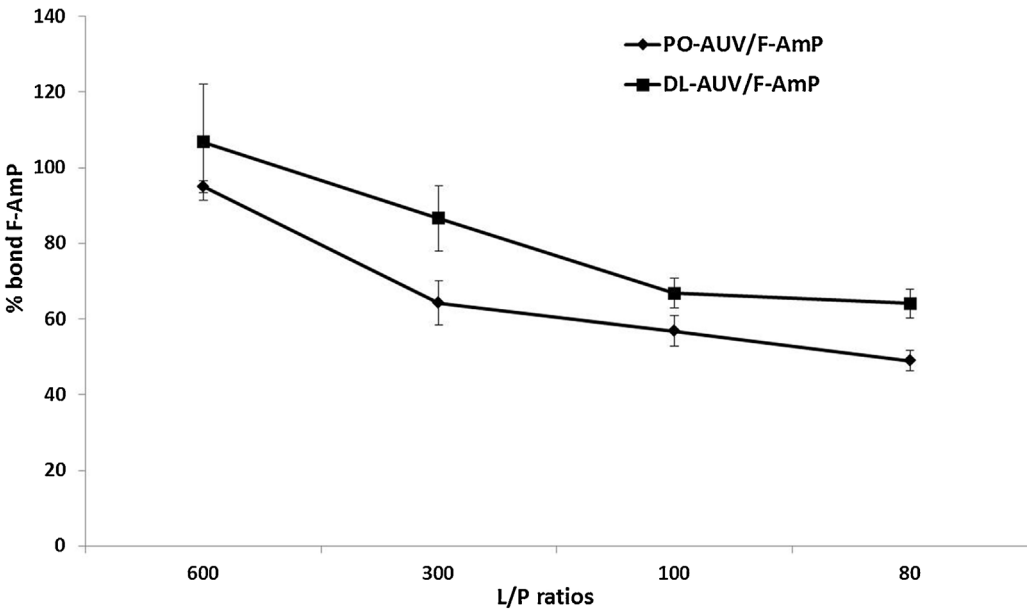

Fig. 5. Quantification of the concentration of F-AmP peptide bound to the liposomes PO-AUVs and DL-AUVs. Plot of the percentage of peptide bound to liposomes towards the L/P mole ratios.

At ratios lower than 60, precipitation started to occur, which can be attributed to liposome clustering.

In order to estimate the number of F-AmP peptide bound to each PO-AUVs, the liposome concentration was measured by using qNano Tunable Resistive Pulse Sensor [42–45]. The number of liposomes (1.80 ± 0.3 E+10) was divided by the total number of peptides bound to the liposomes. It was found that the number of peptides bound to each liposome increases from around 3000 at L/P ratio 600 to around 11000 peptides at L/P ratio 80.

Considering a surface area of 45,216 nm^2 for the 120 nm diameter liposome and the area occupied by the peptide in either a parallel (39,000 nm^2) or a perpendicular (16,000 nm^2) orientation with respect to the liposome, the percentage of occupied area by the peptides on each liposome would be more than 40%. These considerations suggest that the action of AMP could be due to both membrane disruption and to blocking of membrane function, or a combination of the two.

3.5.5. *Shape factor by AF4-MALS-DLS system*

Finally, the gyration diameter of the complexes was measured by AF4-MALS and the results compared with the ones coming from the AF4-DLS, thus allowing us to calculate the resulting shape factors (Table 3).

In order to have information regarding the particle shape [33], we calculated the shape factor $\rho = R_G/R_H$ for all liposome complexes at the peak maximum of the LS 90° signal. From the data in Table 3 we can conclude that all samples have a shape factor close to 1, which is typical of coated sphere morphology. This provides indications that the binding of the peptide to the liposomes does not disturb the original morphology of the liposomes. However a change towards shape factors smaller than unit was noticed for the larger complex in the DL-AUVs/F-AmP system at both 100:1 and 80:1 ratios. This shows that the morphology of the liposome-peptide complex keeps a spherical shape, and the slightly reduced shape factor for the biggest DL-AUVs/F-AmP indicates a more homogeneous mass distribution, suggesting the formation of multilamellar liposomes. Cationic peptides can bridge like-charged membranes and, as a consequence, favor the conversion into a multilamellar phase [46]. In order to confirm the formation of multilamellar vesicles, dispersion of DL-AUVs alone and mixed with F-AmP at 80:1 were analyzed by negative staining Transmission Electron Microscopy for enhanced detail and morphological investigations. **Fig. A-4** A and B shows negative stained DL-AUVs of a wide size distribution ranging from 80 nm to 200 nm. The majority of these appear as unilamellar vesicles. In the presence of AmP at 80:1 L:P ratio (A-4C and D) multilamellar structures were apparent, while the shape of some liposomes appeared distorted. This effect might be due to both the high vacuum conditions needed to operate the electron microscope and the osmotic shock of liposomes during the staining process (interaction between the sample and the uranyl acetate in water solution). Although this technique seems still not well optimized for studying the real size and morphology

Table 3
Geometric diameter (d_G) calculated from AF4-MALS data using the coated sphere fitting mode and hydrodynamic diameter (d_H) determined from AF4-DLS of liposomes alone and mixed with F-AmP peptide. The shape factor ρ is given by R_G/R_H.

	Liposome alone	600:1	300:1	100:1	80:1
PO-AUV/F-AmP	131.0 ± 0.2 (d_G) 125.6 (d_H) $\rho = 1.04$	127.8 ± 0.1 (d_G) 125.2 (d_H) $\rho = 1.02$	129.8 ± 0.2 (d_G) 125.4 (d_H) $\rho = 1.03$	127.2 ± 0.2 (d_G) 120.1 (d_H) $\rho = 1.06$	123.8 ± 0.1 (d_G) 121.6 (d_H) $\rho = 1.02$
DL-AUV/F-AmP	108.4 ± 0.1 (d_G) 114.1 (d_H) $\rho = 0.95$	107.6 ± 0.1 (d_G) 112.6 (d_H) $\rho = 0.96$	106.2 ± 0.1 (d_G) 110.7 (d_H) $\rho = 0.96$	102.2 ± 0.2, 157.4 ± 0.2 (d_G) 112.4, 191.0 (d_H) $\rho = 0.91, 0.82$	104.4 ± 0.2, 176.4 ± 0.3 (d_G) 113.0, 202.3 (d_H) $\rho = 0.92, 0.87$

of liposomes, it is good enough to confirm the presence of multilamellar liposomes.

4. Conclusions

The AF4 multidetection system used in this study enabled the determination of accurate particle size distribution and provided an unprecedented level of characterization for studying liposome – peptide interactions. The use of online DLS and MALS measurements allowed to both measure the unbiased size of particles after continuous and non-destructive particle separation and to gain information on their shape and morphology by detecting their shape factor. Using this information it was possible to identify subtle differences in complexes between positively charged F-AmP peptide with both the negatively charged PO- and DL-AUVs. While in the first case, the complex was composed of a single population with a similar size as the PO-AUVs alone and coated sphere morphology, in the latter we identified, in addition to the "normal" complex, a second complex with a larger size and a perturbed spherical morphology. This unprecedented level of insights highlights the potential of the techniques that we have developed and is a clear reminder of the intrinsic weaknesses of measuring size of popydispersed samples using DLS in batch mode. Furthermore, the online coupling of the UV and fluorescence detectors enables one to directly quantify the amount of bound peptides to each liposome.

The application of this method to study other liposome systems would be quite straightforward, and it is reasonable to assume that this method will be very useful in studying liposome–peptide (and even proteins) interaction in the search for therapeutic peptides. In fact, liposomes are of particular interest because of their potential as drug delivery system, but attention has to be given to their separation as they are porous and pressure-sensitive. The described methodhas clear advantages in this regard as it does not break, agglomerate, or alter liposomes while eluting.

Acknowledgment

The work was funded by the European Community's Seventh Framework Programme, ERA-NET Plus, under Grant Agreement No. 217257.

Appendix A. Supplementary data

Supplementary data associated with this article can be found, in the online version, at http://dx.doi.org/10.1016/j.chroma.2015.10.029.

References

[1] M.R. Mozafari, Nanoliposomes: preparation and analysis, Methods Mol. Biol. 605 (2010) 29–50.
[2] D.D. Lasic, Liposomes: From Physics to Applications, Elsevier, Amsterdam/New York, 1993.
[3] T.M. Allen, Drug delivery systems: entering the mainstream, Science 303 (2004) 1818–1822.
[4] V.P. Torchilin, Recent advances with liposomes as pharmaceutical carriers, Nat. Rev. Drug Discov. 4 (2005) 145–160.
[5] H.-I. Chang, M.-K. Yeh, Clinical development of liposome-based drugs: formulation, characterization, and therapeutic efficacy, Int. J. Nanomed. 7 (2012) 49–60.
[6] J. Giddings, Field-flow fractionation: analysis of macromolecular, colloidal, and particulate materials, Science 260 (1993) 1456–1465.
[7] B. Schmidt, K. Loeschner, N. Hadrup, A. Mortensen, J.J. Sloth, C.B. Koch, E.H. Larsen, Quantitative characterization of gold nanoparticles by field-flow fractionation coupled online with light scattering detection and inductively coupled plasma mass spectrometry, Anal. Chem. 83 (2011) 2461–2468.
[8] B. Roda, A. Zattoni, P. Reschiglian, M.H. Moon, M. Mirasoli, E. Michelini, A. Roda, Field-flow fractionation in bioanalysis: a review of recent trends, Anal. Chim. Acta 635 (2009) 132–143.
[9] P. Reschiglian, A. Zattoni, B. Roda, E. Michelini, A. Roda, Field-flow fractionation and biotechnology, Trends Biotechnol. 23 (2005) 475–483.
[10] R. Qureshi, W. Kok, Application of flow field-flow fractionation for the characterization of macromolecules of biological interest: a review, Anal. Bioanal. Chem. 399 (2011) 1401–1411.
[11] C. Cascio, D. Gilliland, F. Rossi, L. Calzolai, C. Contado, Critical experimental evaluation of key methods to detect, size and quantify nanoparticulate silver, Anal. Chem. 86 (2014) 12143–12151.
[12] K.A. Brogden, Antimicrobial peptides: pore formers or metabolic inhibitors in bacteria? Nat. Rev. Microbiol. 3 (2005) 238–250.
[13] C.D. Fjell, R.E.W. Hancock, A. Cherkasov, AMPer: a database and an automated discovery tool for antimicrobial peptides, Bioinformatics 23 (2007) 1148–1155.
[14] S. Grau, G. Bou, E. Fondevilla, J. Nicolás, M. Rodríguez-Maresca, L. Martínez-Martínez, How to measure and monitor antimicrobial consumption and resistance, Enfermed. Infec. Microbiol. Clín. 31 (Suppl. 4) (2013) 16–24.
[15] J.L. Fox, Antimicrobial peptides stage a comeback, Nat. Biotechnol. 31 (2013) 379–382.
[16] C.D. Fjell, J.A. Hiss, R.E.W. Hancock, G. Schneider, Designing antimicrobial peptides: form follows function, Nat. Rev. Drug Discov. 11 (2012) 37–51.
[17] J.A.F. Opdenkamp, Lipid asymmetry in membranes, Annu. Rev. Biochem. 48 (1979) 47–71.
[18] L. Ryan, B. Lamarre, T. Diu, J. Ravi, P.J. Judge, A. Temple, M. Carr, E. Cerasoli, B. Su, H.F. Jenkinson, G. Martyna, J. Crain, A. Watts, M.G. Ryadnov, Anti-antimicrobial peptides: folding-mediated host defense antagonists, J. Biol. Chem. 288 (2013) 20162–20172.
[19] R. Pecora, S.R. Aragón, Theory of light scattering from hollow spheres, Chem. Phys. Lipids 13 (1974) 1–10.
[20] J.H. Van Zanten, H.G. Monbouquette, Characterization of vesicles by classical light scattering, J. Colloid Interface Sci. 146 (1991) 330–336.
[21] T. Blessing, J.-S. Remy, J.-P. Behr, Monomolecular collapse of plasmid DNA into stable virus-like particles, Proc. Natl. Acad. Sci. 95 (1998) 1427–1431.
[22] H. Binder, K. Gawrisch, Effect of unsaturated lipid chains on dimensions, molecular order and hydration of membranes, J. Phys. Chem. B 105 (2001) 12378–12390.
[23] D.D. Lasic, Liposomes in Gene Delivery, CRC Press, 1997.
[24] L. Calzolai, D. Gilliland, C.P. Garcìa, F. Rossi, Separation and characterization of gold nanoparticle mixtures by flow-field-flow fractionation, J. Chromatogr. A 1218 (2011) 4234–4239.
[25] P.J. Wyatt, Submicrometer particle sizing by multiangle light scattering following fractionation, J. Colloid Interface Sci. 197 (1998) 9–20.
[26] W. Burchard, Light Scattering from Polymers, Springer-Verlag, Berlin, 1983, pp. 1–124.
[27] N.C. Santos, M.J.E. Prieto, A. Morna-Gomes, D. Betbeder, M.A.R.B. Castanho, Structural characterization (shape and dimensions) and stability of polysaccharide/lipid nanoparticles, Biopolymers 41 (1997) 511–520.
[28] W. Burchard, Static and Dynamic Light Scattering from Branched Polymers and Biopolymers, vol. 48, Springer, Berlin/Heidelberg, 1983, pp. 1–124.
[29] P.A. Fuierer, B. Li, H.S. Jeon, Characterization of particle size and shape in an ageing bismuth titanate sol using dynamic and static light scattering, J. Sol–Gel Sci. Technol. 27 (2003) 185–192.
[30] M. Baalousha, F.V.D. Kammer, M. Motelica-Heino, H.S. Hilal, P. Le Coustumer, Size fractionation and characterization of natural colloids by flow-field flow fractionation coupled to multi-angle laser light scattering, J. Chromatogr. A 1104 (2006) 272–281.
[31] B. Chu, T. Liu, Characterization of nanoparticles by scattering techniques, J. Nanopart. Res. 2 (2000) 29–41.
[32] D. Kunz, A. Thurn, W. Burchard, Dynamic light scattering from spherical particles, Colloid Polym. Sci. 261 (1983) 635–644.
[33] O. Wattraint, I. Saadallah, V. Silva-Pires, P. Sonnet, C. Sarazin, Influence of the insertion of a cationic peptide on the size and shape of nanoliposomes: A light scattering investigation, Int. J. Pharmaceut. 454 (2013) 621–624.
[34] A.B. Jessica Lohrke, Karsten Mäder, Characterization of superparamagnetic iron oxide nanoparticles by asymmetrical flow-field-flow-fractionation, Nanomedicine: Nanotechnol. Biol. Med. 3 (2008) 437–452.
[35] S. Hupfeld, D. Ausbacher, M. Brandl, Asymmetric flow field-flow fractionation of liposomes: optimization of fractionation variables, J. Sep. Sci. 32 (2009) 1465–1470.
[36] M.G. Ryadnov, G.V. Mukamolova, A.S. Hawrani, J. Spencer, R. Platt, RE coil: an antimicrobial peptide regulator, Angew. Chem. Int. Ed. 48 (2009) 9676–9679.
[37] P. Rakowska, J. Haibo, R. Santanu, P. Alice, B. Lamarre, M. Carr, P.J. Judge, J. Ravi, U.I.M. Gerling, B. Koksch, G.J. Martyna, B.W. Hoogenboom, A. Watts, J. Crain, C.R.M. Grovenor, M.G. Ryadnov, Nanoscale imaging reveals laterally expanding antimicrobial pores in lipid bilayers, PNAS 10 (2013) 8918–8923.
[38] B.J. Berne, R. Pecora, Dynamic Light Scattering: With Applications to Chemistry, Biology, and Physics, Dover Publications, Mineola, NY, 2000.
[39] V.M. Gun'ko, A.V. Klyueva, Y.N. Levchuk, R. Leboda, Photon correlation spectroscopy investigations of proteins, Adv. Colloid Interface Sci. 105 (2003) 201–328.
[40] M. Kaszuba, D. McKnight, M.T. Connah, F.K. McNeil-Watson, U. Nobbmann, Measuring sub nanometre sizes using dynamic light scattering, J. Nanopart. Res. 10 (2007) 823–829.
[41] E. Sevcsik, G. Pabst, A. Jilek, K. Lohner, How lipids influence the mode of action of membrane-active peptides, Biochim. Biophys. Acta – Biomembr. 1768 (2007) 2586–2595.
[42] D. Kozak, W. Anderson, R. Vogel, M. Trau, Advances in resistive pulse sensors: devices bridging the void between molecular and microscopic detection, Nano Today 6 (2011) 531–545.

[43] G.R. Willmott, M.F. Broom, M.L. Jansen, R.M. Young, W.M. Arnold, Tunable elastomeric nanopores, in: O. Hayden, K. Nielsch (Eds.), Molecular- and Nano-Tubes, Springer US, 2011, pp. 209–261.
[44] G.S. Roberts, D. Kozak, W. Anderson, M.F. Broom, R. Vogel, M. Trau, Tunable nano/micropores for particle detection and discrimination: scanning ion occlusion spectroscopy, Small 6 (2010) 2653–2658.
[45] G.S. Roberts, S. Yu, Q. Zeng, L.C.L. Chan, W. Anderson, A.H. Colby, M.W. Grinstaff, S. Reid, R. Vogel, Tunable pores for measuring concentrations of synthetic and biological nanoparticle dispersions, Biosens. Bioelectron. 31 (2012) 17–25.
[46] L. Moshe, G. Saper, O. Szekely, Y. Linde, C. Gilon, D. Harries, U. Raviv, Modulating the structure and interactions of lipid-peptide complexes by varying membrane composition and solution conditions, Soft Matter 9 (2013) 7117–7126.